

# CAPABILITIES AND PERFORMANCE OF S-BAND SEMI-ACTIVE MULTI-STATIC SMALL SAR CONSTELLATION FOR THE EQUATORIAL REGION

Abdul Duane Lawal<sup>(1)</sup>, Radice, Gianmarco<sup>(2)</sup>

<sup>(1)</sup> Space Glasgow, College of Engineering, University of Glasgow, G12 8QQ,  
[a.lawal.1@research.gla.ac.uk](mailto:a.lawal.1@research.gla.ac.uk)

<sup>(2)</sup> Space Glasgow, College of Engineering, University of Glasgow, G12 8QQ,  
[Gianmarco.Radice@glasgow.ac.uk](mailto:Gianmarco.Radice@glasgow.ac.uk)

**Abstract:** *The attractiveness of flying several Synthetic Aperture Radar (SAR) satellites in a semi-active configuration has been proposed by several studies. The closest implementation of such a mission scenario is exemplified by the current TerraSAR-X and Tandem-X mission, where both spacecraft are identical monostatic platforms capable of operating in various modes. The Bistatic operation mode of the Tandem-X mission is a basic form of the semi-active Multi-static operation mode where one satellite serves as a transmitter while the other records the scattered signals simultaneously. The use of a typical monostatic SAR spacecraft operating in-tandem with several receiver only spacecraft is a semi-active mode of operation. This paper examines the capabilities of implementing a constellation of S-band spaceborne SAR platform for alongtrack interferometry over the Equatorial Region for velocity measurement with particular focus on ship detection. The proposed orbit for the mission is a low inclined circular low Earth orbit, which ensures high revisit time, quick coverage and high data throughput. The pendulum orbital configuration is adopted to maintain the relative distance between successive SAR platforms. The conditions and constraints necessary to achieve the orbit geometry required to conduct alongtrack interferometry are defined. The alongtrack separation between platforms necessary to measure specified ship velocity is also discussed. Finally an error budget estimate of the measure radial velocity is provided.*

*Keywords: Alongtrack Interferometry, SAR, Equatorial Region, Radial Velocity*

## 1. Introduction

The benefits of spaceborne SAR interferometry are currently being demonstrated by recent and planned future missions [1-6]. SAR interferometry is a remote sensing technique capable of providing data to understand various natural phenomena on Earth. Generally speaking, SAR interferometry involves the use of the phase differences in the same transmitted signal, received at two different locations to compute additional information about the imaged terrain [16]. The computed information is useful in generating maps of digital elevation models. Specifically, alongtrack SAR interferometry provides means of detecting moving targets within the view scene of the sensors, and allowing velocity measurements of these targets.

Alongtrack SAR interferometry has a distinction which provides a substantial advantage over conventional optical sensors mainly due to its all weather, day/night, high resolution capabilities analogous to conventional monostatic SAR. One application area is in sea surface observations to investigate phenomenon such as wave spectra and ocean currents on the basis of superficial velocity distributions. It has been used to improve measurements from conventional SAR data as well as understand the nature of SAR imaging of ocean waves and surface [6 - 11]. Furthermore, a plethora of operational applications areas such as fisheries management, warning on potential hazards to human and marine life, observation of internal gravity waves as well as surveillance of surface slicks or films such as oil spills have been investigated [12].

The all-weather/light capability of a SAR system and the desire for a high rate revisit time over a pre-defined coverage area informs the use of a space-borne SAR interferometric configuration. Furthermore, the requirement for a low cost mission dictates the investigation of a multistatic configuration of spaceborne SAR satellites [13], with a typical monostatic spacecraft (transmitter/receiver) and several passive spacecraft (receiver-only), for the alongtrack interferometric operations. The pre-defined coverage area is located within the tropical region and defined by the geographical latitudes  $\pm 10^\circ$  both side of the Equator and called the *Equatorial Region* (ER). The pendulum formation has been used as the operational paradigm as it does not inherently cause an alongtrack separation [13-17], thereby keeping the distances between spacecraft relatively uniform throughout the orbit. The selected operating frequency is the S-band with a wavelength of 0.15m. In contrast to most recent SAR missions which utilize either the X-band or C-band frequencies [20–22] for operation, this mission adopts an approach similar to the proposed Surrey Satellite Technology Limited (SSTL) NovaSAR mission which uses S-band frequency [18, 19 & 25]. Considering the dense atmospheric environment of the ER due to regular, heavy rainfall, the need for high penetrating ability is a key factor for selection of the wavelength. Furthermore, longer wavelength provides larger critical baseline ( $B_C$ ), and less stringent control requirements for operating a set of formation flying spacecraft performing interferometric operations [13 & 15].

This work is structured to investigate the capabilities and performance of a constellation of S-band SAR microsatellites for interferometric applications by monitoring illegal bunkering activities within the ER. The task includes demonstrating the capability of alongtrack interferometry for detecting moving targets and measuring velocity component along the line-of-sight (LOS). The paper also addresses the peculiarity of the orbit design to meet the mission objectives, with main focus on trajectory synchronisation of the SAR antennas. Finally, error budget analysis of the accuracy of the radial velocity measurement is presented. For the purpose of clarity, a simple twin “leader/follower” configuration is illustrated.

## 2. Orbit Geometry

SAR interferometry is a technique that relies on the phase difference obtained from the same transmitted signal, and received from two different spatial locations, to compute information about the imaged observation [14]. For alongtrack interferometry, the relative position of each spaceborne carrying SAR antenna is an important factor that ensures consistency in the data acquired. Alongtrack interferometry basically involves the acquisition of a SAR image by two antennas under identical geometry of observation, separated in time [26]. The time separation between both antennas is proportional to the level of correlation between each image captured by each antenna. Therefore, a shorter interval of time between both antennas prevents the effect of decorrelation on the phase measurement accuracy [27], which is an established limitation for differential SAR interferometry [28]. The phase difference ( $\psi_{12}$ ) between signals reflected from the same target is a resultant of variation in slant range (R) from the antenna [26]. The resulting interferometric phase resulting from the co-registered complex SAR images is given by: [26]

$$\psi_1 = -\frac{2\pi}{\lambda} 2R_1(t) \quad (1)$$

$$\psi_2 = -\frac{2\pi}{\lambda} 2R_2(t + \Delta t) \quad (2)$$

$$\psi_{12} = \frac{4\pi}{\lambda} (V_{rad}\Delta t) \quad (3)$$

Where  $\psi_1$  is the phase of the signal received at the first SAR antenna and  $\psi_2$  is the phase of the signal received at the second antenna from the same imaged observation.  $\psi_{12}$  is the phase difference between pixels representing the same target on each captured image which forms the interferograms,  $t$  is the initial time the first SAR signal hits the desired imaged observation,  $\Delta t$  is the time difference due to the difference in anomaly angle of both SAR carrying antennas,  $R_1(t)$  and  $R_2(t+\Delta t)$  are the slant ranges to the same observed target,  $\lambda$  is the selected radar wavelength;  $V_{rad}$  is the line-of-sight velocity vector component of the target velocity and called the radial velocity of the target. Since the target radial velocity is the desired measurement, it can be calculated from;

$$V_{rad} = \frac{1}{\Delta t} \left( \frac{\lambda}{4\pi} \psi_{12} \right) \quad (4)$$

This is based on the assumption of an ideal geometry of observation where both spaceborne SAR satellites orbit the same trajectory and have similar pointing with respect to the target area [29]. Practically, however, it is not possible to ensure that both spaceborne SAR satellites follow the same path while orbiting, due to effects of orbit perturbations and in other cases incorrect antenna pointing. This shortcoming results in a deviation between the orbits of the spaceborne SAR, leading to an interferometric baseline (B) as seen (Figure 1(b)). Also evident from Figure 1(b) is the resulting slant range differences  $R_1(t)$  and  $R_2(t + \Delta t)$ , implying non-zero interferometric phase measurement even when the target is stationary. In order to

reduce the effects of false measurements, the “non-zero interferometric phases” must be removed to retrieve the correct target velocity measurements [26].

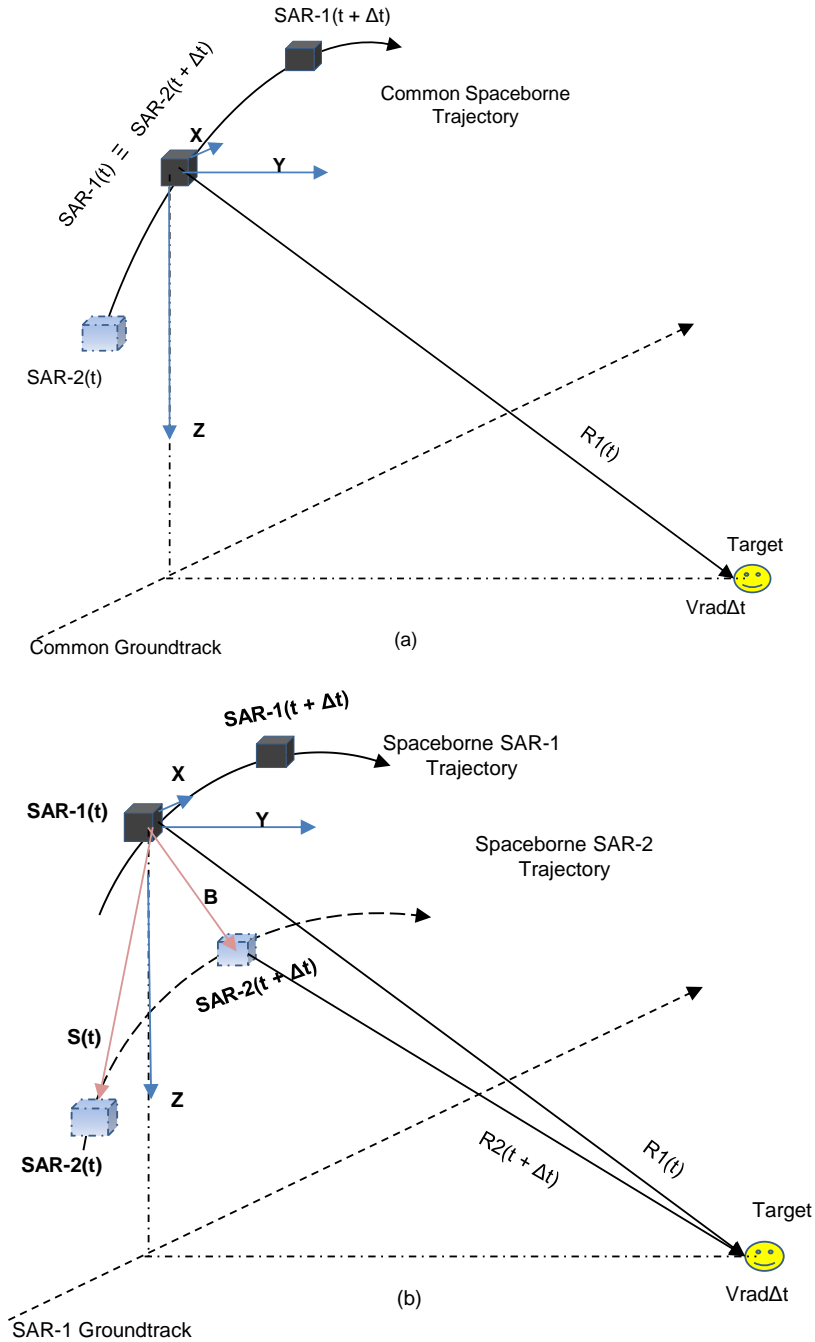


Figure 1. Spaceborne SAR Configuration for Alongtrack Interferometric Operation in  
(a) Ideal case (b) Perturbed case

Neglecting antenna pointing errors, and accounting for the non-zero base line case, the phase difference ( $\psi_{12}$ ) must be modified to give:

$$\psi_{12} = \frac{4\pi}{\lambda} [R_1(t) - R_2(t + \Delta t)] = \frac{4\pi}{\lambda} \psi_{12} (B_z \cos\theta - B_y \sin\theta) \quad (5)$$

$$V_{rad} = \frac{1}{\Delta t} \left( \frac{\lambda}{4\pi} \psi_{12} - B_z \cos\theta - B_y \sin\theta \right) \quad (6)$$

Where  $\theta$  represents the SAR antenna look angle,  $B_y$  and  $B_z$  are the components of the interferometric baseline vector  $B$  defined by the orbit reference frame (ORF) of the antenna on SAR-1 spacecraft (Figure. 2)

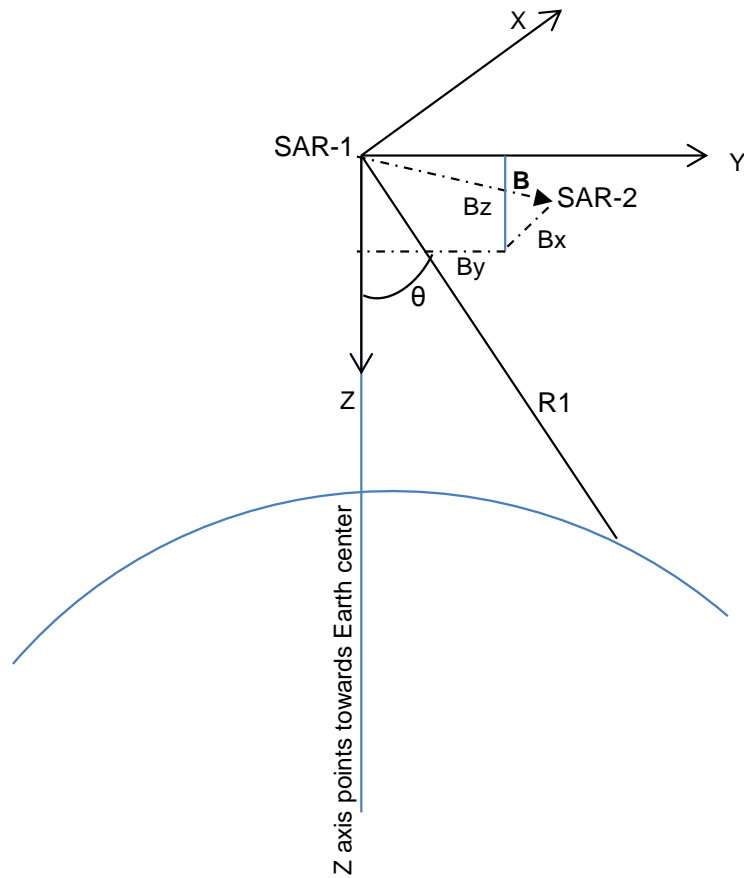


Figure 2. Orbit reference frame and interferometric baseline

For the purpose of brevity, a similar configuration has been extensively discussed by [26] where a detailed description of the ORF can be found so it will not be repeated here. In addition, [26] also discusses the requirements for avoiding the need for at least one ground control point to enable phase unwrapping, even though there is high a correlation for alongtrack SAR interferometry due to simultaneous observations. The possibility is dictated by the constraint of ensuring the interferometric phase contribution does not exceed  $2\pi$  and leading to the identification of a time separation  $\Delta t$  to be maintained during operations as a function of the maximum measurable radial velocity  $V_{rad}$ . Based on the assumption that  $V_{rad}$  varies in the interval  $[-V_{max}, V_{max}]$ , and using (4), the contributions of the interferometric phase difference is limited to the interval  $[-\pi, \pi]$ , to prevent the ambiguity in the  $V_{rad}$  sign whenever the time separation  $\Delta t$  is given by [26]

$$\Delta t_n = \frac{\lambda}{4V_{max}} \quad (7)$$

### 3. Pendulum Configuration for S-Band Spaceborne Alongtrack Interferometry

To adequately design the orbit trajectory for spaceborne SAR, one must duly account for Earth rotation. Generally speaking, platform orbital dynamics is usually described in the Earth centre inertial (ECI) reference frame; however it is paramount to describe the spaceborne SAR orbit an Earth-fixed rotating reference frame (ERF) to directly detect range variations and relative velocities.

To ensure that all the spacecraft flying in formation have the same groundtrack with a constant time separation that ensures interferometric operations, they must all be placed in a circular orbit with identical semi-major axis ( $a$ ) and inclination ( $i$ ). This can be achieved by meeting the conditions of selecting the appropriate value for the right ascension of ascending node (RAAN) and true anomaly values within the selected orbital plane. The spacecraft positions at initial time  $t_0$  when SAR-1 is crossing the RAAN are shown in Figure 3. The future time  $t_f$  it takes for SAR-2 to arrive the ascending node is defined by  $\Delta t$  from above.

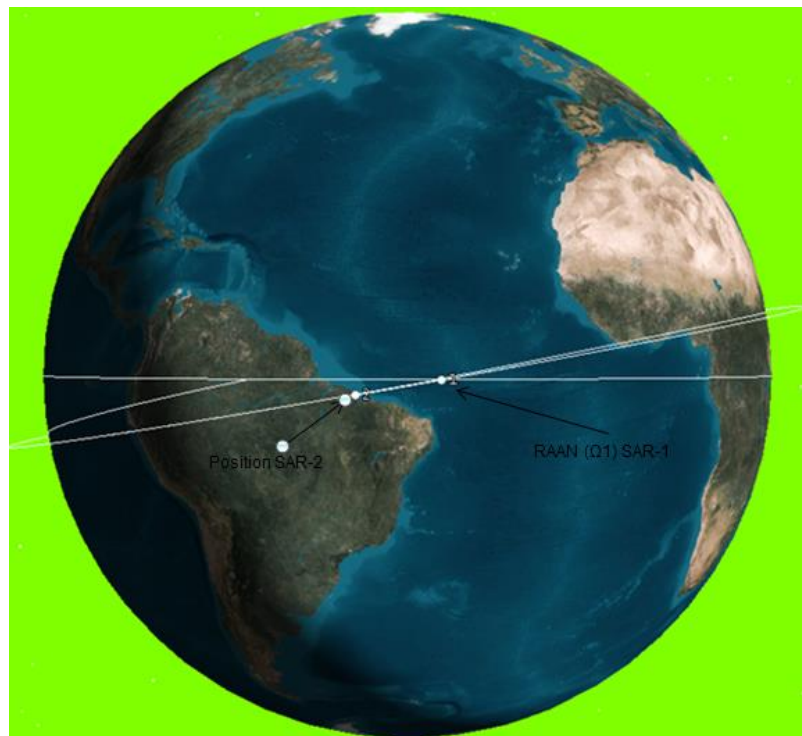


Figure 3. Spacecraft configuration at RAAN of SAR-1

To meet these conditions, it is paramount to ensure that the ratio of RAAN differences ( $\Delta\Omega$ ) between spacecraft in formation, with the Earth rotation rate ( $\Omega_E$ ) are equal to the time separation value ( $\Delta t_n$ ). Furthermore, the same time separation value must also be equal to the ratio of the difference between the anomaly values and the orbit precession rate ( $\omega_o$ ). These conditions can be met by assuming [26]:

- The Z-axis of the ECI reference frame is coincident with both the  $Z_E$ -axis of the ERF reference frame and the Earth rotation axis

- The X-axis of the ECI reference frame is aligned along the vernal equinox
- The Xe-axis of the ERF reference frame points towards the spacecraft ascending node

$$\frac{\Omega_2 - \Omega_1}{\Omega_E} = \frac{v_1 - v_2}{\omega_o} = \Delta t_n \quad (8)$$

From Eq. 8 it can be noticed that SAR-2 crosses each parallel of latitude at  $\Delta t_n$  seconds after SAR-1, and since the Earth rotates equal angles in equal interval of time, the groundtrack of both spaceborne SAR are the same as long as the  $\Delta\Omega$  at the ascending nodes is equal to the product of the Earth rotation rate and time separation ( $\Omega_E \Delta t_n$ ).

It is assumed that the rates of change for the mean motion ( $\dot{M}$ ), perigee precession ( $\dot{\omega}$ ) in the orbital plane and the ascending node precession ( $\dot{\Omega}$ ) in the RAAN plane are constant for a low Earth orbit (LEO) [26]. To determine the separation components of the baseline vector, we define SAR-1 orbit reference frame (ORF) with the vector  $x_o, y_o, z_o$ , and origin at the center of SAR-1 antenna (see Figure 4). The benefit of the ORF is the ease of locating spacecraft relative position along the orbits.

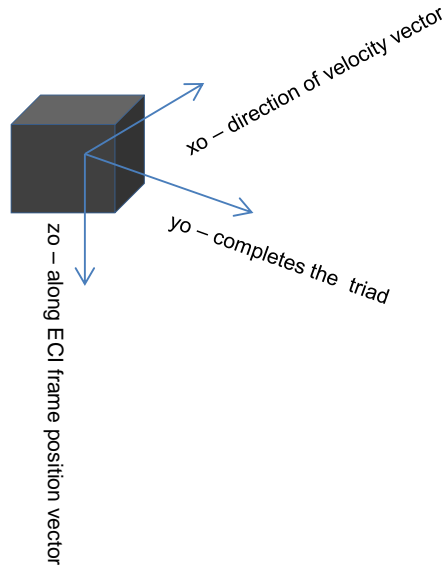


Figure 4. Spacecraft ORF define by vectors  $x_o, y_o, z_o$

A detailed procedure of ensuring the groundtrack of both spaceborne SAR platforms coincide can be seen in [26]. Assuming,  $\mathbf{S}$  as the relative position vector between both spacecraft antennas, its components  $S_{x_o}$ ,  $S_{y_o}$  and  $S_{z_o}$  are the alongtrack, across-track and vertical separation distances respectively.  $S_{x_o}$  and  $S_{z_o}$  remain constant along the orbit, with  $S_{x_o}$  depends on the selected time separation and the orbital parameters. Conversely, the  $S_{y_o}$  component is constantly varying throughout

the orbit due to the relative change in position between the spaceborne SAR platform and maximum separation experienced at the nodes.

#### 4. Mission Scenario

The proposed mission scenario adopts the pendulum configuration as a requirement for conducting spaceborne SAR interferometry. To this end, several papers have been presented [30, 31, and 32] to establish the stability of the relative motion between spacecraft [30] and determine the control requirement for the formation [32]. From the previous section, it can be noted that designing the geometry necessary for conducting alongtrack interferometry, exhibits similar characteristics to the pendulum configuration.

The mission is specifically tasked to monitor the radial velocities of ships within and around the ER to assist in detecting illegal marine activities such as oil bunkering or illegal oil ballast discharge. Ship detection can assist in providing information to government and law enforcement agencies, environmental protection agencies, agencies that monitor ship traffic and coast guard for search and rescue operations [19]. Ships are detected as a bright point against the ocean background [19]. A typical sea-faring cargo vessel travels at an average speed ranging between 14 Knots and 24 knots [33]. However, the act of conducting illegal activities within territorial waters occurs with ships moving at much lower speeds. This work will therefore investigate the minimum separation distance between spaceborne SAR platform required to detect ship speed of 0.514 m/s (1 Knot).

The Spaceborne SAR platform operates at a wavelength of 0.1m from an altitude of 700km, in a Keplerian circular orbit, with all conditions required to ensure spacecraft groundtrack coincide are satisfied. Table 1 shows the baseline orbital parameters required to measure the radial velocity ( $V_{rad}$ ) of a ship moving at 0.52m/s. Using Eq. 7, the time separation  $\Delta t_n$  between the spaceborne SAR platforms is approximately 0.0486s.

Table 1. Orbit parameters of Spaceborne SAR platform

Parameters	SAR-1	SAR-2	Delta parameters
Semi-major axis (m)	7078140	7078140	0
Eccentricity (deg)	0	0	0
Inclination (deg)	0	0	0
RAAN ( $\Omega$ ) (deg)	10.0000	10.0002	0.0002
True anomaly (deg)	10.0000	9.99996	0.000049

Figure 5 shows the ORF components of  $\mathbf{S}$  for the specified case of  $\Delta t_n = 0,0486$  s.



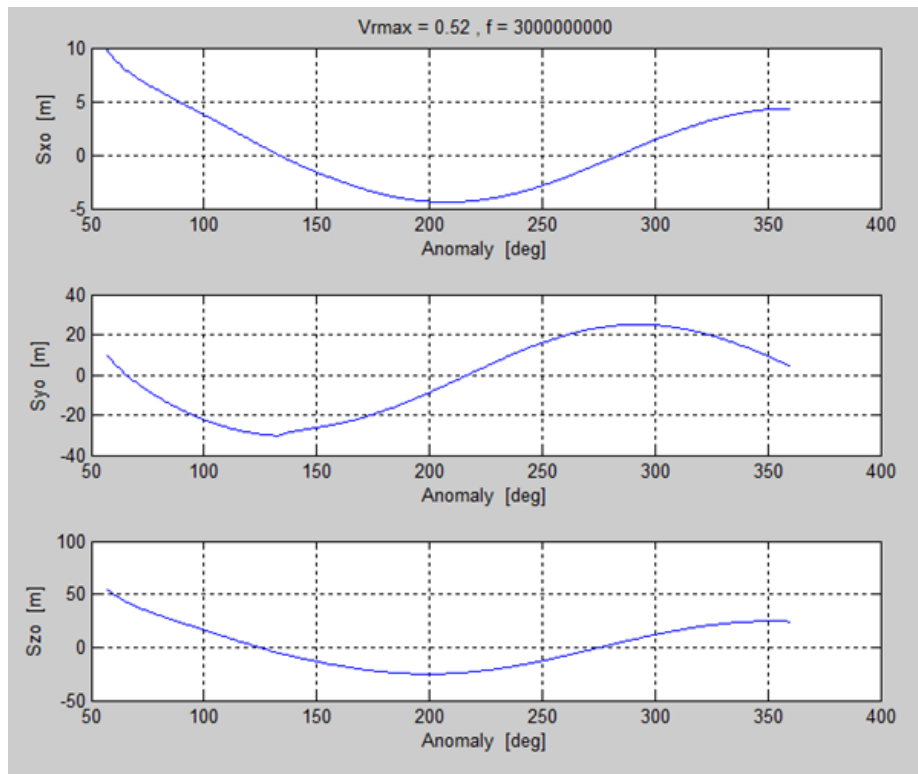


Figure 5. Spacecraft separation ORF components in case of S-band SAR radar

To better understand the effects of time separation ( $\Delta t_n$ ) with respect to maximum radial velocity ( $V_{rmax}$ ), Figure 6 shows a plot of  $\Delta t_n$  vs  $V_{rmax}$  at various wavelengths using orbital parameter values consistent with those provided in Table 1.

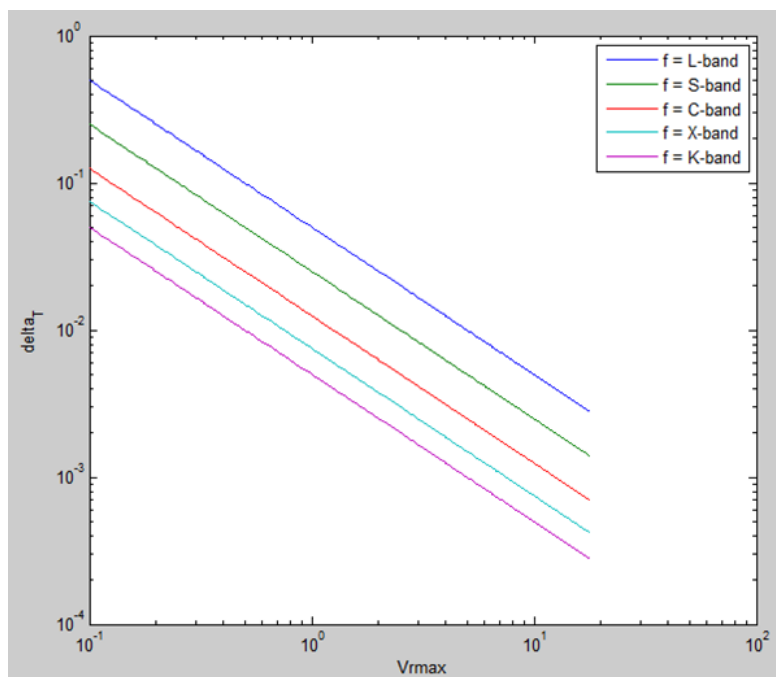


Figure 6. Nominal time separation as a function of maximum measurable target radial velocity for several wavelengths

## 5. Radial Velocity Measurement Accuracy Error Budget

To estimate the error budget of the radial velocity measurement accuracy, a worse-case scenario is adopted by assuming that Eq. 4 yields:

$$\frac{\lambda}{4\pi} |\psi_{12}| \gg |B_z \cos \theta + B_y \sin \theta| \quad (9)$$

It is evident that these condition cannot be easily met as described in [26], therefore, Eq. (6) is used to conducted a quantitative error budget for the accuracy, where the time separation is assumed to be [26],

$$\Delta t = \frac{s_v}{V} = \frac{\lambda}{4V_{rmax}} \quad (10)$$

Where  $S_v$  is the component of  $\mathbf{S}$  along the velocity vector and  $V$  is the magnitude of SAR-2 spacecraft velocity in the ERF. Assuming a look angle  $\theta$  of  $45^\circ$ , the slant range can be expressed as follows

$$R = (Re + H) \cos \theta - \sqrt{(Re + z)^2 - (Re + H)^2 \sin^2 \theta} \quad (11)$$

where  $Re$ ,  $H$  and  $z$  are the Earth radius, orbit height and the average height to be measured respectively as shown on Figure. 7.

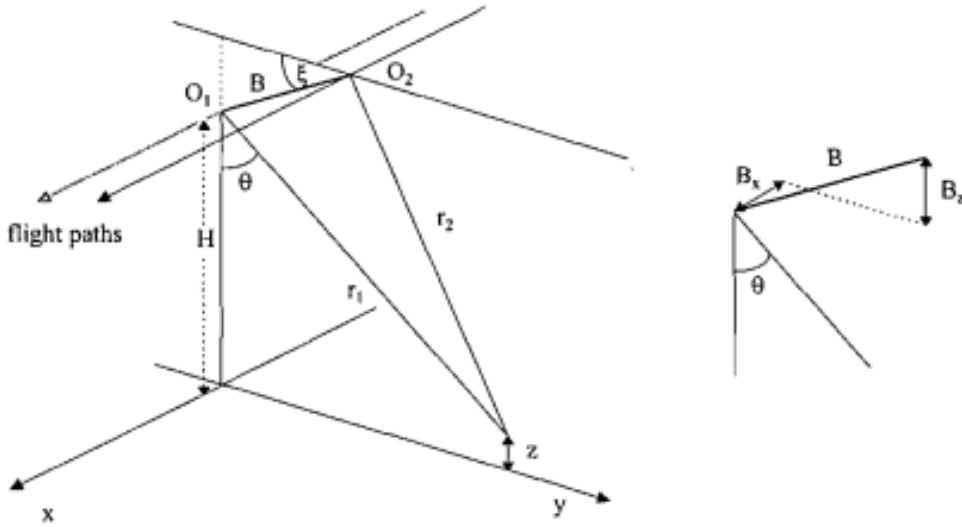


Figure 7. Principal SAR Interferometry Geometry [34]

By differentiating Eq. 6, Eq. 10 and Eq. 11, the first order estimate of the errors in  $V_{rad}$  due to uncertainties in the parameters can be obtained [26]. Based on the assumptions of uncorrelated parameters [35], the total uncertainties for the measurement are given by:

$$\sigma_{Vrad}^2 = \left(\frac{V_{rad}}{\partial V}\right)^2 \sigma_V^2 + \left(\frac{\partial V_{rad}}{\partial s_v}\right)^2 \sigma_{s_v}^2 + \left(\frac{V_{rad}}{\partial h}\right)^2 \sigma_h^2 + \left(\frac{V_{rad}}{\partial B_z}\right)^2 \sigma_{B_z}^2 + \left(\frac{V_{rad}}{\partial B_y}\right)^2 \sigma_{B_y}^2 + \left(\frac{V_{rad}}{\partial \psi_{12}}\right)^2 \sigma_{\psi_{12}}^2 + \left(\frac{V_{rad}}{\partial R}\right)^2 \sigma_R^2 + \left(\frac{V_{rad}}{\partial a}\right)^2 \sigma_a^2 \quad (12)$$

A detailed calculation of each value of uncertainty can be seen in [26], however, for the purpose of brevity, only the measured radial velocity uncertainty as a function of signal-to-noise ratio (SNR) of the interferometric pair and baseline control accuracy will be discussed.

From Eq. 12,  $\sigma_V, \sigma_{S_V}, \sigma_h, \sigma_{B_z}, \sigma_{B_y}, \sigma_{\psi_{12}}, \sigma_R, \sigma_a$  are the uncertainties expected from the measurement of spaceborne SAR-2 velocity, alongtrack separation component, height, baselines z and y components, phase difference, slant range and orbit semi major axis.

As mentioned previously, the worse-case is assumed as:

$$V_{rmax} \cong \frac{V}{S_V} \left( \frac{\lambda}{4\pi} \psi_{12} - B_z \cos\theta - B_y \sin\theta \right) \quad (13)$$

$$B_y \cong B_z \cong B_{max} = \max\{|B_y| | B_z|\} \quad (14)$$

with  $B_{max}$  representing a non-zero value of the baseline components which is permitted by the control system for ground track repetition and referred to as the baseline control error. To enable clarity, all velocity measurement accuracy are been divided to  $V_{rmax}$  to get dimensionless values in the graphs. Typical values from Table 1 are used, with an incidence angle of  $45^\circ$  and the operational number of looks ( $N_L$ ) of 4. The calculated velocity of spaceborne SAR-2 is 7500 m/s and the interferometric pair correlation ( $\gamma$ ) dependent on SNR is given by Eq. 16, while from [16], a typical SNR value of 20db is assumed.

The error estimate of the interferometric phase noise for distributed targets is given by: [36]

$$\sigma_{\psi_{12}} = \frac{1}{\sqrt{2N_L}} \frac{\sqrt{1-\gamma^2}}{\gamma} \quad (15)$$

$$\gamma = \frac{SNR}{1+SNR} \quad (16)$$

The measurement accuracy expressed as a function of SNR for several numbers of looks is shown in Figure. 8. From Figure 8, an increase in the number of looks improves the accuracy of the measurement although the error contributed small.

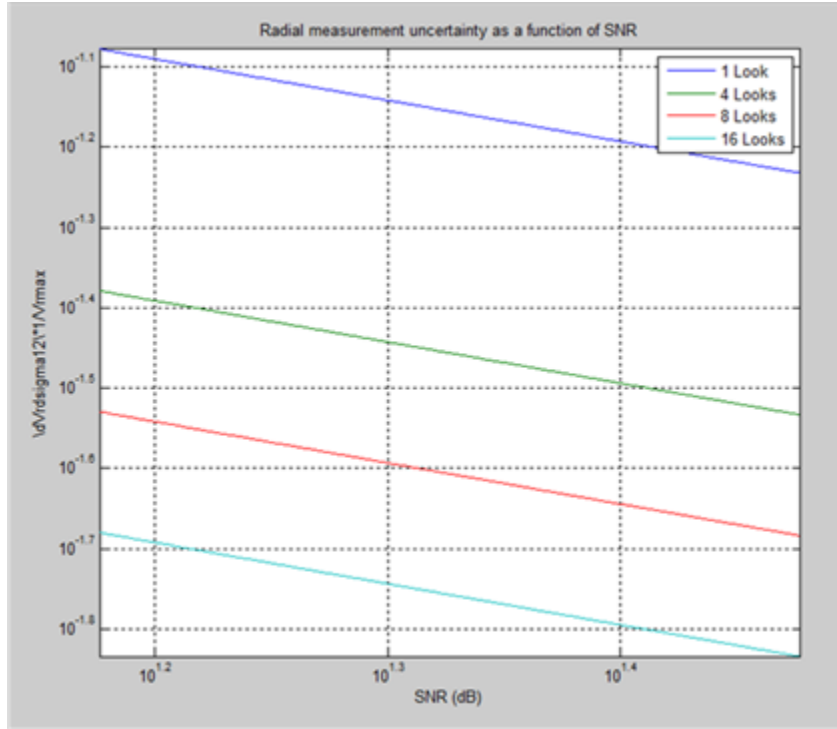


Figure 8. Radial velocity measurement uncertainty as a function of SNR of interferometric image pair

The maximum error in baseline control with respect to radial velocity measurement accuracy can also be represented by the relationship:

$$\left| \frac{\partial V_{rad}}{\partial h} \right| \frac{\sigma_h}{V_{rmax}} \cong \frac{4R_E}{\lambda R a} \left( 1 + \frac{1}{\tan \theta} \right) B_{max} \sigma_h \quad (17)$$

For this study, it is assumed that the measurement is performed with reference to the model of the marine geoid and hence the value of  $\sigma_h$  adopted is 10m [37]. The plot on Figure 9 shows the effects of the measured error and how critical it is to the alongtrack interferometric measurement. It is also useful for defining the orbit control requirements for the spaceborne SAR platform.

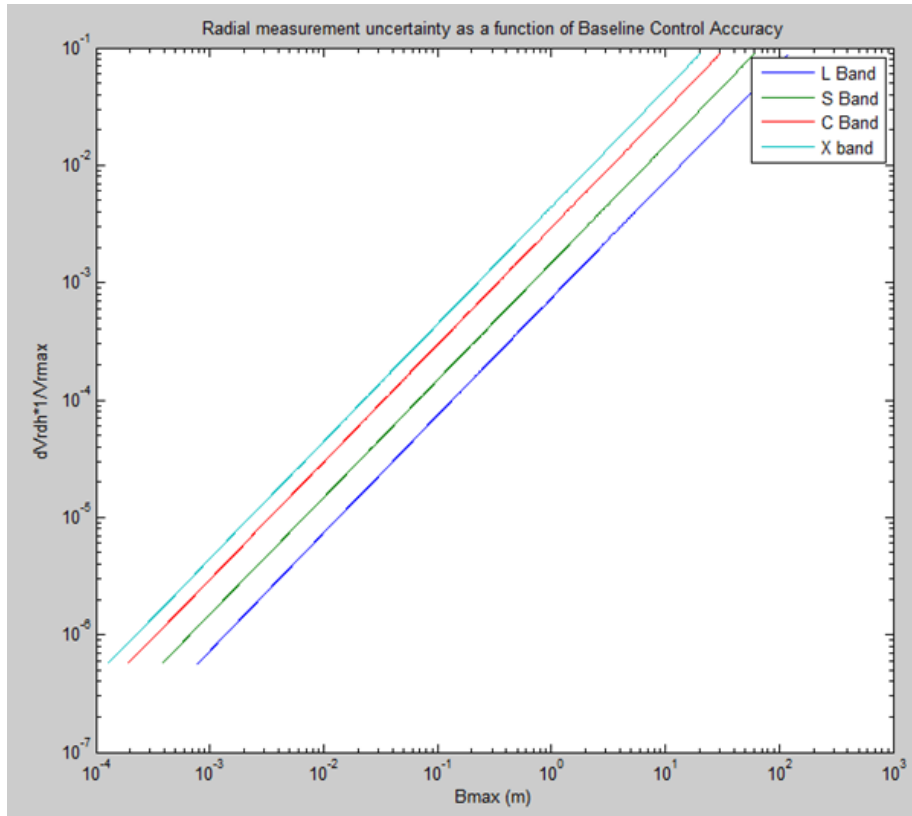


Figure 9. Radial velocity measurement uncertainty as a function of baseline control accuracy.

## 5. Conclusions

Several studies have investigated the capabilities of using alongtrack SAR interferometry for GTMI applications by measuring target velocity component along line of sight. Commonly reported is the successful use of airborne systems in most cases. Although, the use of spaceborne along-track interferometry has received growing attention from both scientific and consumer communities, it is still being exploited as it is yet to deliver on its promising potentials. Typically, the benefits of spaceborne SAR interferometry would include its ability to provide global coverage. However, this paper presents a proposed system of spaceborne SAR interferometry dedicated to the Equatorial Region. The system is devoted to detecting the marine activities of sea going vessels by conducting velocity measurements across the observed scenario. The configuration of the proposed orbit formation has been addressed, with focus on ensuring that the trajectories all spaceborne antennas used for vessel velocity measurement are with respect to the rotating Earth reference frame.

Specific constraints that ensure that the groundtrack of both platforms coincide to enable the implementation of alongtrack interferometry have been presented. Particular attention was given to the nature of the proposed mission and the effects of varying the alongtrack separation distance as a function of radar wavelength was discussed.

A few of the possible errors in estimating the measured radial alongtrack velocities were highlighted. Results of the effects of radial velocity measurement errors as a function of baseline control and SNR were also presented.

In summary, measuring ship velocity of 1 knot within the ER can be a demanding mission dictated by the choice of radar wavelength. However the results presented show that it is possible to implement such a mission once all the potential sources of errors are accounted for.

## 6. References

- [1] Moreira, A., Hajnsek, I., Krieger, G., Papathanassiou, K., Eineder, M., De Zan, F., Younis, M., Werner, M., "Tandem-L: Monitoring the Earth's Dynamics with InSAR and Pol-InSAR," PolinSAR 2009, Frascati, Italy, January 2009
- [2] Massonnet, D., and Rabaute, T., "Radar interferometry: Limits and potential," IEEE Trans. Geosci. Remote Sensing, vol. 31, pp. 455-464, Mar. 1993
- [3] Bernhard Rabus, Michael Eineder, Achim Roth, Richard Bamler, "The shuttle radar topography mission—a new class of digital elevation models acquired by spaceborne radar", ISPRS Journal of Photogrammetry and Remote Sensing, Volume 57, Issue 4, February 2003, Pages 241-262
- [4] Thompson, A. A., and Livingstone, C. E., "Moving target performance for RADARSAT-2", IGARSS 2000, Honolulu
- [5] Bamler, R., and Hartl, P., "Synthetic aperture radar interferometry", Inverse Problems 14, 1998
- [6] Jao, J. K., "Theory of Synthetic Aperture Radar Imaging of a Moving Target", IEEE Trans. Geosci. Remote Sensing, vol. 39, no. 9, pp. 1984-1992, 2001.
- [7] Goldstein, R. M., Li, F., Smith, J., Pinkel, R., and Barnett, T. P. (1994) "Remote sensing of ocean waves: The surface wave process program experiment". Journal of Geophysical Research, 99, C4 (1994), 7945—7950
- [8] Milman, A. S., Scheffler, A. O., and Bennett, J. R. (1992) "Ocean imaging with two-antenna radars". IEEE Transactions on Antennas and Propagation, 40 (1992), 597—605
- [9] Shemer, L., and Marom, M. (1993) "Estimates of ocean coherence time by an interferometric SAR". International Journal of Remote Sensing, 14, 16 (1993), 3021—3029.

- [10] Carande, R. E. (1994) "Estimating ocean coherence time using dual-baseline interferometric synthetic aperture radar". IEEE Transactions on Geoscience and Remote Sensing, 32, 4 (1994), 846—854.
- [11] Shemer, L. (1993) "Interferometric SAR imagery of a monochromatic ocean wave in the presence of real aperture radar modulation". International Journal of Remote Sensing, 14, 16 (1993), 3005—3019.
- [12] Evans, D. L. (Ed.). (1995) "Spaceborne Synthetic Aperture Radar: Current Status and Future Directions". NASA/TM-4679, 1995
- [13] Krieger, G., Wendler, M., Fiedler, H., Mittermayer, J., Moreira, A., "Comparison of the Interferometric Performance for Spaceborne Parasitic SAR Configurations", EURSAR 2002, Koln 4-6 June 2002
- [14] Willis, N., "Bistatic Radar", Artech House, Boston, 1991
- [15] Fiedler, H., Krieger, G., Jochim, F., Kirschner, M., and Moreira, A., "Analysis of satellite configurations for spaceborne SAR interferometry," in Int. Symp. Formation Flying Missions & Tech., Toulouse, France, 2002
- [16] Zebker, H. A., and Villasenor, J. (1992) "Decorrelation in interferometric radar echoes". IEEE Transactions on Geoscience and Remote Sensing, 30, 5 (1992), 950—959
- [17] Peterson, E and Zee, R.E "Possible Scenarios for an InSAR Formation Flying Microsatellite Mission" Proceedings of the 22nd Annual AIAA/USU Conference on Small Satellites, Logan, UT, USA, Aug. 11-14, 2008, SSC08-VI-5
- [18] Philip Whittaker, Martin Cohen, David Hall, Rachel Bird, Luis Gomes, "NovaSAR – A Novel, Low Cost, Medium Resolution Spaceborne SAR System Development," Proceedings of the 3rd Workshop on Advanced RF Sensors and Remote Sensing Instruments (ARSI), Noordwijk, The Netherlands, Sept. 13-15, 2011.
- [19] Philip Davies, Alex da Silva Curiel, Rachel Bird, Philip Whittaker, Martin Cohen, David Hall, Luis Gomes, "Changing the Radar paradigm – Technology and cost trades in establishing the NovaSAR constellation," 6th International Conference 'Remote Sensing- the Synergy of High Technology,' Moscow, Russia, April 25-27, 2012,"
- [20] Fox, P. "The RADARSAT-II Mission," Proceedings of IGARSS'99, Hamburg, Vol. III, June28 - July 2, 1999, pp. 1500-1502
- [21] Krieger, G., Moreira, A., Hajnsek, I., Werner, M., Fiedler, H., Settelmeier, E. "The TanDEM-X Mission Proposal," Proceedings of the ISPRS Hannover Workshop 2005, Hannover, Germany, May 17-20, 2005

- [22] Krieger, G., Moreira, A., Hajnsek, I., Werner, M., Fiedler, H., “TanDEM-X: Mission Concept and Performance Analysis,” Proceedings of IGARSS 2005, Seoul, Korea, July 25-29, 2005
- [23] Ulaby F.T., R. Moore, and A.K. Fung, Microwave Remote Sensing (Volume 1,2,3), Addison Wesley, Reading (MA), 1981, 1982, 1986. – Advanced
- [24] Oliver C. and S. Quegan, Understanding Synthetic Aperture Radar Images, ArtechHouse, 1998. - Basic to Advanced
- [25] Alpers W. et al. “Comparison of ocean wave imaging by ERS-1 and ALMAZ-1 synthetic aperture radar”. Roc. 2nd ERS-I Symposium, Hamburg, Germany, 11-14 Oct. 1993, v.1, p.239-245
- [26] Moccia, A., Rufino, G., “Spaceborne Along-Track SAR Interferometry: Performance Analysis and Mission Scenarios”, IEEE Trans. Aerospace Electronic Systems, Vol. 37, No. 1, pp. 199-213, 2001.
- [27] Zebker, H. A., and Villasenor, J. (1992) “Decorrelation in interferometric radar echoes”. IEEE Transactions on Geoscience and Remote Sensing, 30, 5 (1992), 950—959.
- [28] Rufino, G., Moccia, A., and Esposito, S. (1998). ” DEM generation by means of ERS tandem data”. IEEE Transactions on Geoscience and Remote Sensing, 36, 6 (1998), 1905—1912.
- [29] Goldstein, R. M., and Zebker, H. A. (1987) “Interferometric radar measurement of ocean surface currents”. Nature, 328 (1987), 707—709.
- [30] Lawal, A and Radice, G. M. “Performance Assessment of an Interferometric SAR Network for the Equatorial Region”. Proceedings of the 63rd IAC (International Astronautical Congress), Naples, Italy, Oct. 1 to Oct. 5, 2012, IAC-12-B4-1.6
- [31] Abdul Lawal, “A Constellation of Distributed SAR Network for Developing Nations” Poster presentation at the ESA (European Space Agency) 4S Symposium, Portoroz, Slovenia, Jun. 1 to Jun. 4, 2012.
- [32] Lawal, A and Radice, G. M. “Control Strategy for Semi-active Multistatic Small SAR Constellation for the Equatorial Region”. Proceedings of the 7<sup>th</sup> International Workshop on Satellite Constellation and Formation Flying (IWSCFF), Lisbon, Portugal, Mar. 13 to Mar. 15, 2013, IWSCFF-2013-08-03
- [33] Nigel Gee “Some New Developments in Container Vessel Design” Report presented by Nigel Gee and Associates 2011
- [34] GENS, R., & VAN GENDEREN, J. I., (1996): “Review Article SAR interferometry—issues, techniques, applications”, International Journal of Remote Sensing, 17:10, 1803-1835



[35] Li, F., and Goldstein, R. M. (1990) “Studies of multi-baseline spaceborne interferometric synthetic aperture radars”. *IEEE Transactions on Geoscience and Remote Sensing*, 28, 1 (1990), 88—97.

[36] Carande, R. E. (1994) “Estimating ocean coherence time using dual-baseline interferometric synthetic aperture radar”. *IEEE Transactions on Geoscience and Remote Sensing*, 32, 4 (1994), 846—854.

[37] Wunsch, C., and Stammer, D. (1998) “Satellite altimetry, the marine geoid, and the oceanic general circulation”. *Annual Rev. Earth Planet Science*, 26 (1998), 219—253